pH-Responsive Thin Film Membranes from Poly(2-vinylpyridine): Water Vapor-Induced Formation of a Microporous Structure

Maxim Orlov,[†] Ihor Tokarev,[†] Andreas Scholl,[‡] Andrew Doran,[‡] and Sergiy Minko*[,†]

Department of Chemistry and Biomolecular Science, Clarkson University, Potsdam, New York 13699, and Lawrence Berkeley National Laboratory, Berkeley, California 94720

Received December 8, 2006; Revised Manuscript Received January 23, 2007

ABSTRACT: We report the fabrication of microporous thin film membranes with two-dimensionally arranged submicron pores whose size can be varied by changing pH of aqueous medium. A solution containing poly(2-vinylpyridine) partially quaternized with 1,4-diiodobutane (qP2VP) and unreacted 1,4-diodobutane (DIB) was used for the formation and deposition of the membranes on solid substrates. The membranes were spin-coated onto solid substrates in a controlled humid environment. The presence of water vapor in air was found to be a necessary condition for the pore formation. We studied the influence of relative humidity on the membrane morphology and proposed a mechanism of pore formation. Cross-linking the qP2VP membranes with DIB made them insoluble (stable) in organic solvents and acidic water. The cross-linked membranes demonstrated pH-dependent swelling, which had a strong influence on the pore size.

Introduction

Microporous polymer membranes (pore size 0.01−20 μm) are widely used in industry, medicine, pharmacology, and research for separation and concentration of particles, colloids, proteins, enzymes, and cells. Phase inversion and track etching are well-established, commercially implemented techniques for the fabrication of such membranes. In the phase inversion technique, a solvent for a polymer turns into a nonsolvent causing the polymer precipitation; the nonsolvent serves as a porogen that evaporates after the membrane formation. Phase inversion is usually achieved by immersion of a solution film into a coagulation bath with a nonsolvent (immersion precipitation), by exposure to nonsolvent vapor, or by temperature change (temperature-induced phase separation). Membranes prepared by this technique exhibit a highly porous inner structure represented by a continuous network of interconnected tortuous pores. Furthermore, the structure is usually asymmetric with a thin dense surface layer and a thick spongelike basic layer. The surface layer determines the separation properties and the overall flow resistance of the membrane, while the basic layer acts as a mechanical support.[1] The track etch (TE) membranes are prepared using a two-step fabrication procedure.[2] First, a polymer film (polycarbonate or polyester) is exposed to a collimated beam of heavy ions that produce parallel tracks across the film. The tracks are then chemically etched, forming cylindrical pores. Unlike the phase inversion membranes, the track etch membranes are characterized by uniform pore size and relatively low pore density, resulting in the high flow resistance.

In addition to the above-mentioned techniques, various template-assisted methods for the fabrication of microporous polymer membranes have been reported in the literature. Colloidal crystals[3−8] and emulsion droplets[9] have been successfully implemented as templates for the fabrication of self-standing membranes. Microcontact molding[10] and casting of polymer layers on solid substrates with 2D pillar arrays[11] were found to be feasible for the fabrication of thin film membranes. An elegant method for the fabrication of membranes with regular pore arrangement is based on controlled drying of a polymer solution cast as a layer on a solid substrate in a highly humid atmosphere.[12−16] Evaporation of a water-immiscible solvent leads to cooling of the solution surface and, consequently, to condensation of a monolayer of hexagonally arranged water droplets that gradually sink into the solution. As the solvent evaporates and the polymer vitrifies, the droplets evaporate leaving pores behind. Polyelectrolyte layer-by-layer assembly[17] and self-assembly of hollow micelles from rod−coil block copolymer[18] represent another nontemplate strategy for the fabrication of microporous layers. The reader interested in the subject can also refer to a recent review by Ulbricht.[19]

Over the past decade, numerous studies were devoted to the fabrication of membranes with variable permeability, specifically, the membranes which pore size can change in response to external stimuli (responsive membranes). Such membranes are of potential interest for a variety of applications, e.g., flow regulation, size- and charge-selective filtration and fractionation, encapsulation of living cells, controlled drug release, and sensors. The common approach for the fabrication of responsive membranes consists of the surface modification (e.g., by graft polymerization) of a premade membrane (usually commercial TE and anodized aluminum membranes as well as membranes fabricated by the phase inversion techniques) with a layer of stimuli-sensitive polymer chains (brush) or a stimuli-sensitive cross-linked polymer network (gel).[20−29] In a few studies,[30−33] responsive membranes were prepared in one step by the immersion precipitation of graft copolymers with stimuli-responsive side chains. The main requirement is that the thickness of the stimuli-sensitive layer has to be comparable with the pore size. Then, the pore permeability will depend greatly on the conformational state of the chains or on the swelling degree of the gel. Responsive membranes in which permeability was dependent on pH[21−25,30,31,33] and/or ionic strength,[21,32] presence of specific ions,[26,31] temperature,[25,27,28] and the strength of an applied electric field[34] have been reported.

Recently, we reported a novel method for the fabrication of responsive polymer gel membranes.[35] The membranes were deposited as thin films on solid substrates from a solution

* Corresponding author. E-mail sminko@clarkson.edu.
[†] Clarkson University.
[‡] Lawrence Berkeley National Laboratory.

10.1021/ma062821f CCC: $37.00
Published on Web 02/27/2007

containing poly(2-vinylpyridine) (P2VP) and 1,4-diodobutane (DIB). It is noteworthy that DIB had a twofold function: it served as a porogen and as a cross-linker for P2VP. Because P2VP is a weak cationic polyelectrolyte, its cross-linked network (gel) demonstrates pH-dependent swelling properties. We observed the reversible contraction of the pores of membranes subjected to acidic water, which was caused by swelling of the P2VP gel. Unlike the responsive membranes previously reported in the literature, the P2VP gel membranes change the pore size by expansion/contraction of their entire body. We demonstrated that the thin film membranes could be easily transferred onto a surface of commercial track etch membranes to produce hybrid membranes with pH-controlled water permeability.

In this paper, we focus on aspects related to the fabrication of the P2VP gel membranes. In particular, we discuss the possible mechanism of the pore formation and demonstrate that humidity is essential for the formation of pores in the P2VP layers.

Experimental Section

Materials. P2VP (M_w = 159 kg/mol) and DIB (99+%, stabilized with copper) were purchased from Aldrich. Nitromethane, dichloromethane, and ammonium hydroxide were purchased from Fisher Scientific, tetrahydrofuran was from EM Science, and hydrogen peroxide, 30%, was from J.T. Baker. All chemicals were analytical grade. 11-Bromoundecyldimethylchlorosilane (BDCS) was received from Gelest, Inc. Highly polished silicon wafers (purchased from Semiconductor Processing Co.) were cleaned in an ultrasonic bath with dichloromethane for 20 min followed by the cleaning solution of NH_4OH:H_2O_2 at 65 °C for 40 min and then rinsed several times with Millipore water.

Sample Preparation. 0.1 g of P2VP and 0.1 mL of DIB were dissolved in a 5 mL solvent mixture consisting of 9 parts of nitromethane and 1 part of tetrahydrofuran. The resulting solution was heated at 60 °C for 2 h while stirring. The heating was necessary to accelerate the quarternization reaction between P2VP and DIB. The reacted solution was cooled down to RT (23 °C) and filtered. Afterward, the solution (called *primary* hereafter) was divided into four equal parts. One part was left intact, while different amounts of extra DIB were added to three others to prepare the solutions with the DIB concentration of 2 (primary), 3, 4, and 6 vol %. The solutions were immediately used for the film deposition. The spin-coating deposition was performed at 3000 rpm with a PM101D Photo Resist Spinner (Headway Research Inc.) installed inside a humidity control chamber (COY Laboratory Products Inc.) held at RT. Films were deposited either onto clean silicon wafers or silicon wafers modified by a BDCS monolayer. The silanization of the silicon wafers was carried out in 1 wt % solution of BDCS in dry toluene for 16 h at RT. The qP2VP films were cross-linked by temperature annealing at 120 °C under vacuum for 48 h. The annealing step also led to covalent binding of the qP2VP films to the BDCS monolayer via quaternization with bromoalkyl end groups.

Instruments. The porous morphology of the qP2VP films was visualized with surface probe microscopy (SPM). We used a Dimension 3100 microscope by Veeco Instruments (Santa Barbara, CA) operating in the tapping mode and BAS-Tap300 Silicon probes (Budget Sensors) with the following characteristics: a tip radius of 10 nm, a spring constant of 40 N/m, and a resonance frequency of 300 kHz. Swelling of the cross-linked qP2VP films in acidic water was studied by carrying out in-situ SPM measurements in a fluid cell. Silicon nitride probes NP (Veeco Instruments) with the radius of 20 nm, the spring constant of 0.32 N/m, and the resonance frequency of ~9 kHz in water were used in the in-situ experiments. SPM topography images were processed by using the Nanoscope III 5.12r2 software provided with the instrument by Veeco Instruments. The particle analysis function allowed us to calculate the size, the depth, and the density of pores; before the analysis the SPM topography images (20 × 20 μm^2) were planarized (first order) and inverted. A SPM scratch analysis was carried out to determine the thickness of the qP2VP films.

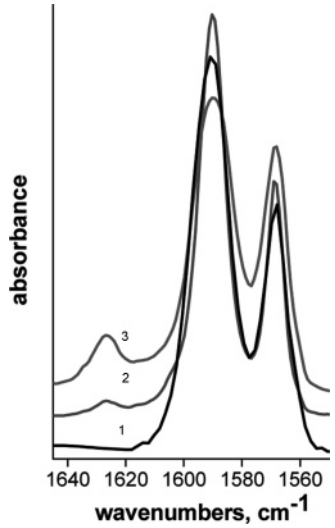

Figure 1. IR spectra of P2VP as is (1), after the quaternization with DIB for 2 h (the quaternization degree 11%) (2), and the subsequent temperature annealing for 48 h (the quaternization degree 23%) (3).

FTIR measurements were carried out with a Vector22 FT-IR spectrometer by Bruker Optics. The absorption band of P2VP at 1590 cm^{-1} (C═C stretching vibrations of a pyridine ring) is strongly affected by the quaternization reaction (Figure 1). Its intensity decreases with a rise in the reaction conversion. At the same time a new absorption band centered at 1627 cm^{-1} evolves. We selected these bands to estimate the fraction of the quaternized pyridine rings (the quaternization degree) in qP2VP. To allow the quantitative analysis, we acquired a calibrating curve by analyzing infrared spectra of micrometer thick films of P2VP (Aldrich), P2VP quaternized with methyl iodide (the quaternization degree was 74% as determined with ^1H NMR), and their mixtures with the mole fractions of 3:1, 1:1, and 1:3. The percentages of the quaternized pyridine rings in the mixtures were 18.5, 37, and 55.5%, respectively. The films for the FTIR measurements were cast from 2 wt % solutions on 1 × 1 cm^2 Si wafers which were polished on both faces. All films, including those cast from the quaternization solutions, were of comparable thickness. The reproducible thickness was obtained by casting the same volume of the polymer solutions of the same polymer concentration in all experiments. The infrared spectra of the Si wafers were measured before the film deposition, and later these spectra were subtracted from the spectra recorded for the samples with the polymer films. The peaks at 1590 and 1627 cm^{-1} were fitted using a Gaussian and Lorentz functions. The plot of relative intensities of the peaks vs the percentages of the quaternized pyridine rings for the pure polymers and their mixtures was used as a calibration curve.

X-ray photoemission electron microscopy (XPEEM) was performed using the PEEM-2 microscope at the beamline 7.3.1.1 of the Advanced Light Source (ALS) synchrotron of the Ernest Orlando Lawrence Berkeley National Laboratory. Samples, thin polymer films deposited on silicon wafers, were irradiated with a monoenergetic X-ray beam at 30° in ultrahigh-vacuum conditions, and the emitted photoelectrons were collected by a system of electrostatic lenses and focused at high magnification onto a detector. Similarly to XPS, the effective sampling depth of XPEEM for polymers does not exceed 10 nm.[36] Near-edge X-ray absorption fine-structure (NEXAFS) spectra of carbon, nitrogen, and oxygen were recorded prior to the XPEEM measurements to determine positions of the resonance peaks of the elements in the samples. XPEEM images of the samples were obtained at photon energies of the incident X-ray radiation, which correspond to the maximum of the resonance peak of an element and to the background (just before the peak). Then, the second image was subtracted from the

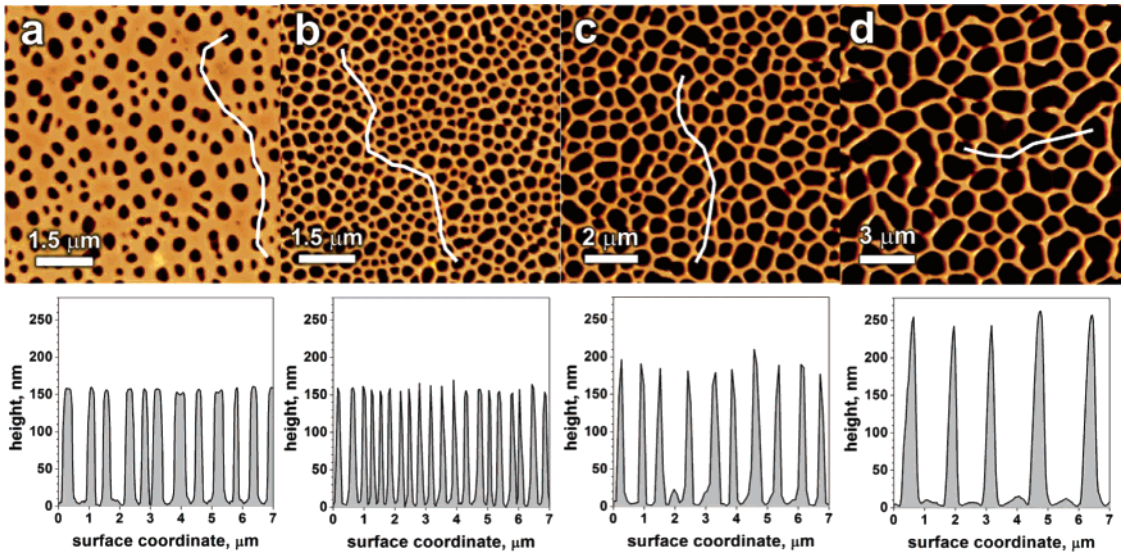

Figure 2. SPM topography images with the corresponding cross-sectional profiles of the qP2VP films spin-coated at 55% RH from the solutions with the DIB concentrations of 2 (a), 3 (b), 4 (c), and 6 vol % (d) onto Si wafers. The quaternization degree of qP2VP is 11%. The lines show the location of the cross-sectional profiles.

Table 1. Average Pore Diameter and the Porosity of the qP2VP Films vs the Volume Content of DIB Acquired from the SPM Topography Images in Figure 1

DIB vol content, %	pore diameter,[a] nm	porosity,[a] %
2	289 ± 158	25
3	268 ± 73	47
4	582 ± 148	60
6	1418 ± 367	67

[a] Measured at half depth of the pores.

first one to yield a differential image showing the surface distribution of the element. The more atoms of a specific element that are detected in a given region, the lighter it appears on the differential or subtracted image.

Results and Discussion

P2VP was quaternized in the presence of an excess of DIB in a 9/1 (v/v) nitromethane/THF solution to the quaternization degree of P2VP of 11% (Figure 1, IR spectrum 1). The quaternization degree approached in the primary solution remained the same even after dissolution of an extra amount of DIB. Since at RT the quaternization reaction is a very slow process, we observed no significant increase in the quaternization degree over the time period required to deposit films for the study. Unreacted DIB evaporated during the spin-coating deposition and the resulting films consisted entirely of qP2VP. Figure 2 presents the SPM topography images of the qP2VP films (150−250 nm thick) spin-coated under ambient conditions (RT of 23 °C and 55% RH) from the solutions with DIB concentrations of 2, 3, 4, and 6 vol %, respectively. All images show the two-dimensional (2D) pattern of isolated concave micropores. The average pore size and the film porosity (Table 1) increase as DIB content grows. The pore size distribution, which is characterized by the standard deviation of the average pore size, decreases from 50% for the film spin-coated from the primary solution to 25−27% for the films spin-coated from the solutions with the higher DIB content.

Examination of the cross-sectional profiles obtained from the SPM images in Figure 2 shows that the pores extend across the film down to the substrate. The continuous pores were also confirmed by the XPEEM measurements. This technique allowed us to visualize the surface distribution of the specific elements in the films. The XPEEM differential images (Figure 3) demonstrated that the signals of carbon and nitrogen, the elements that are present in qP2VP, were received from the polymer film. No signals of those elements were observed in the pores' area. At the same time the signal of oxygen, the element that is present in the native oxide film of a Si wafer substrate, was clearly detected in the pores' area. Although the XPEEM data show no qP2VP on the pore bottoms, the presence of an adsorption layer of the polymer cannot be excluded.

We found that humidity has a strong influence on the morphology of spin-coated films. Figure 4 shows the SPM topography images of the qP2VP films (150−165 nm thick) spin-coated from the primary solution in a humidity range from 30 to 75%. The average size and depth of the pores (Table 2) decrease significantly when the relative humidity (RH) is lowered. This is accompanied by an increase in the surface pore density (Table 2) and a broadening of the pore size distribution. The average pore depth is equal to the film thickness for the films spin-coated at a relative humidity of 55% (Figure 2a) and higher, indicating that most of pores extend across the film down to the substrate. Conversely, the film spin-coated at 30% RH exhibits the skin-deep pores (15 nm average depth). The intermediate situation is observed for the film deposited at 45% RH.

In a control experiment, we spin-coated the films from a solution containing only qP2VP. The solution was prepared as follows: qP2VP was precipitated from the primary solution, washed thoroughly to remove the unreacted DIB, dried under vacuum, and then redissolved in the 9:1 mixture of nitromethane and THF to form 2 wt % solution. The spin-coated films were smooth and featureless over the whole humidity range. This experiment provides evidence that pores were not produced by condensed water droplets as had been observed in previous studies for some systems at high humidity.[12−16] Therefore, the pore formation is caused by liquid−liquid phase separation in the qP2VP/DIB solutions into qP2VP-rich and DIB-rich phases. Furthermore, we found that the presence of even small amounts of water in the solution can significantly affect the solubility of DIB. Specifically, DIB has unlimited solubility in the 9/1 (v/v) mixture of dry nitromethane and THF, while its solubility lowers to 11 vol % upon the addition of 1% water (which is close to the water solubility limit at RT). On the basis of this fact, we may speculate that absorption of water can be

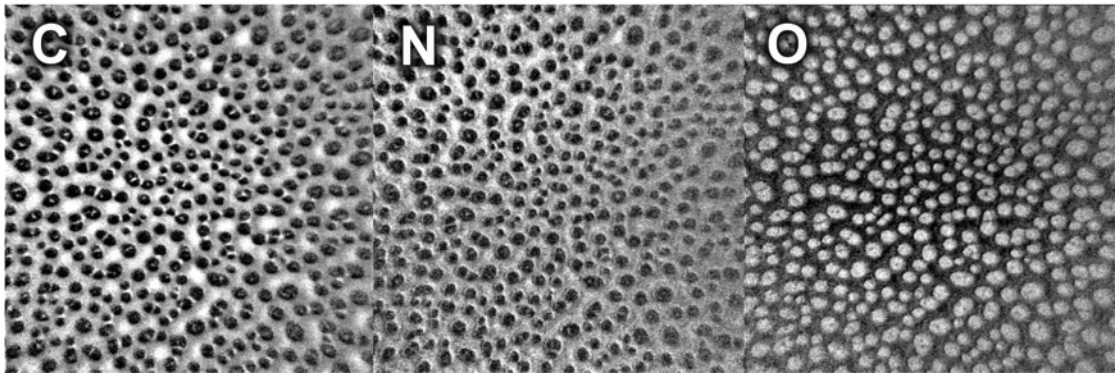

Figure 3. Characteristic XPEEM differential images of the qP2VP film showing the surface distributions of C, N, and O. The images' size is 20 × 20 μm^2. The lighter the area on the images, the stronger is the signal from a specified element.

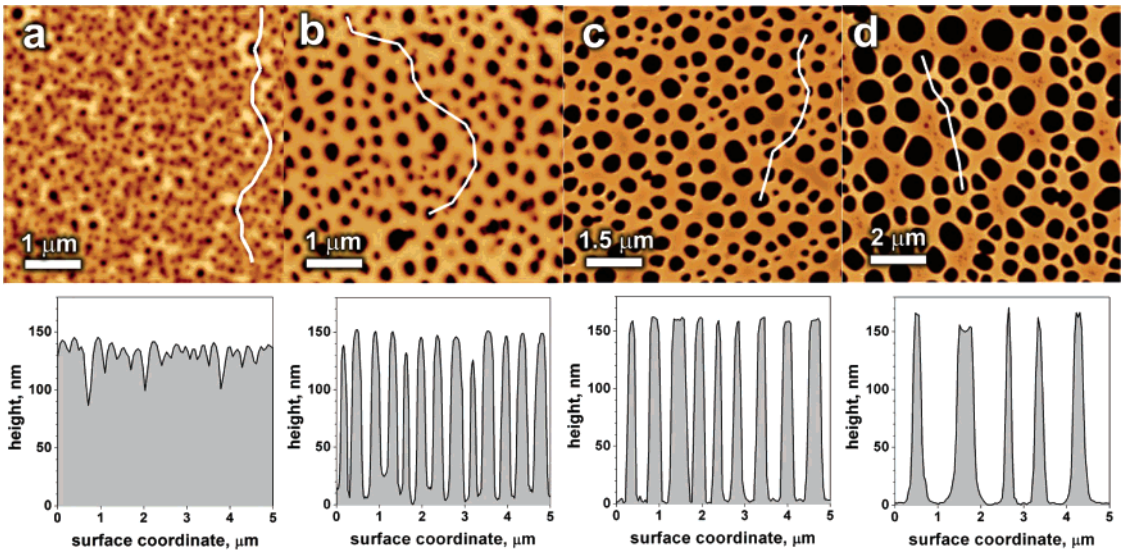

Figure 4. SPM topography images with the cross-sectional profiles of qP2VP films spin-coated from the primary solution at RH of 30% (a), 45% (b), 60% (c), and 75% (d) onto Si wafers. The quaternization degree of qP2VP is 11%. The lines show the locations where the profiles were obtained.

Table 2. Average Depth, Average Diameter, and Density of the Pores of the qP2VP Films vs Relative Humidity Set during the Spin-Coating Deposition of the Films (Calculated from the SPM Topography Images in Figure 4)

RH, %	pore depth, nm	pore diameter,[a] nm	surface pore density, μm^{-2}
30	15 ± 7	84 ± 42	16.2
45	136 ± 18	169 ± 63	6.7
60	159 ± 8	346 ± 93	2.8
75	165 ± 5	601 ± 204	1.1

[a] Measured at half depth of the pores.

responsible for the phase separation of a solution during the spin-coating.

In view of the findings noted above, the following scenario of the pore formation was proposed. Initially, a homogeneous qP2VP/DIB solution is spread over a substrate surface by centrifugal forces (Figure 5A). The concentrations of qP2VP and DIB in the solution rapidly rise due to solvent evaporation. This is accompanied by a lowering of the solution temperature and by water condensation when the dew point is reached. Condensed water mixes with the solution, thus lowering the DIB solubility. As the DIB concentration exceeds the solubility limit, the solution undergoes the phase separation. Obviously, the time needed to reach the dew point depends significantly on the relative humidity. According to the Magnus−Tetens formula,[37] at 75% RH the dew point is 18.2 °C, which is close to RT and therefore can be reached quickly. Conversely, the dew point at 30% RH is as low as 3.3 °C, indicating that at low humidity the water condensation may not occur at all. Hence, the phase separation occurs at a late stage, when most of the solvent is evaporated. As DIB phase separates, it forms droplets on the surface (Figure 5B). The droplets' formation can be rationalized by the high DIB/water interfacial energy. To illustrate this, we measured the contact angles of a DIB drop on a continuous qP2VP film in air and under water. The obtained values differed noticeably, being 10° and 75°, respectively. The continuous solvent evaporation maintains the supersaturation state, which is necessary for the formation of new droplets and for the growth of the already existing droplets. Another mechanism responsible for the droplets' coarsening is coalescence. An indication of this coalescence can be easily seen from the images in Figure 2b−d. It is noteworthy that, because the viscosity of the solution increases as the solvent evaporates, the mobility of the droplets decreases. It explains why the droplets do not sink into a layer in the films spin-coated at low humidity.

As the solvent evaporates, qP2VP vitrifies and "freezes" the formed microstructure of the DIB droplets (Figure 5C). The film formation is completed by the evaporation of slowly volatile DIB, which leaves the pores behind (Figure 5D).

Earlier phase separation provides sufficient time for the growth of droplets. The concentration of DIB in the solution and the relative humidity are the main factors that determine

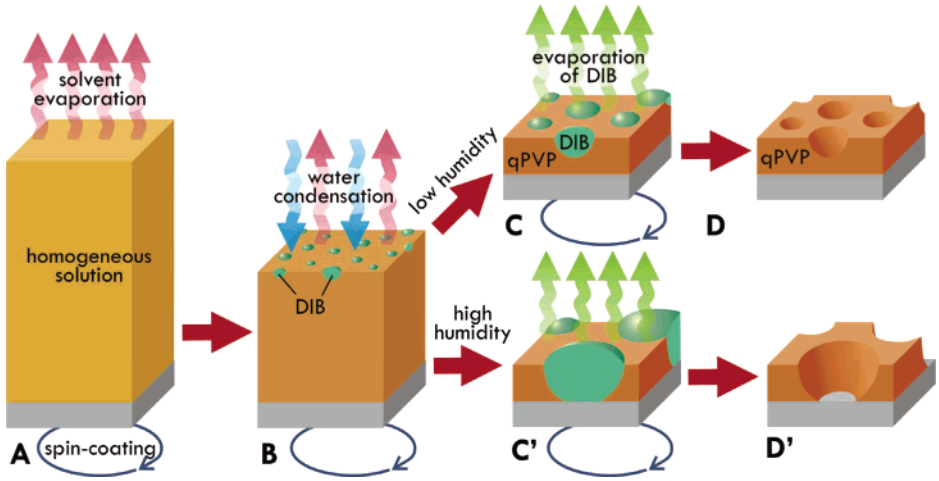

Figure 5. Sketch showing different stages in the pore formation process: (A) a thin film of a homogeneous qP2VP/DIB solution spread by centrifugal forces over a rotating substrate, (B) solvent evaporation followed by water condensation and the formation of DIB droplets, (C) qP2VP vitrification followed by DIB evaporation, and (D) a resulting porous qP2VP film. (C, D) <55% RH and (C′, D′) >55% RH.

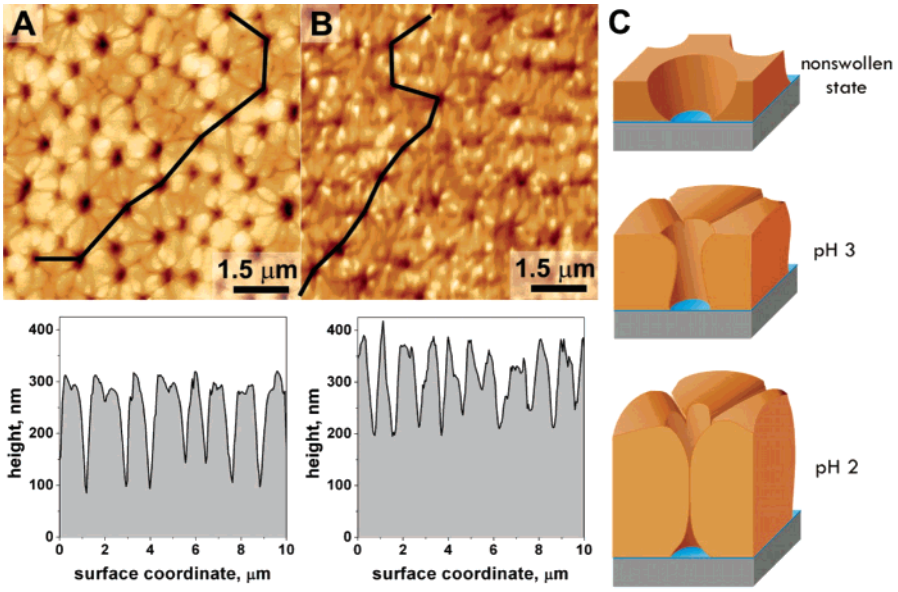

Figure 6. (A, B) SPM topography images with the corresponding cross-sectional profiles of the cross-linked qP2VP film under acidic water of pH 3 (A) and pH 2 (B). The film was spin-coated at RH of 55% from the solution with the DIB concentration of 2 vol % onto a Si wafer modified with a BDCS monolayer and annealed at 120 °C under vacuum for 48 h. The quaternization degree of qP2VP after the temperature annealing is 23%. The lines show the location of the cross-sectional profiles. (C) Sketch showing the cross-sectional profiles of a membrane's pore in the dry and swollen states.

the moment when the supersaturation occurs. Another factor that affects the final size of pores is the quaternization degree. This statement is based on two observations. The films spin-coated from a solution containing nonquaternized P2VP and DIB (taken in the same amounts as in the primary solution) exhibit notably smaller pores as compared to those shown in Figure 4. The films spin-coated from the aged solutions (stored for days) always exhibit the larger pore size as compared to those shown in Figure 4. As we have already mentioned, the quaternization reaction takes place even at RT, although this process is very slow. Thus, the qP2VP quaternization degree rises with storage time. The growth in the quaternization results in an increase in hygroscopicity of P2VP, and thus, a shorter amount of time is needed to reach the supersaturation state.

We would like to note the difference between the above process of pore formation and the well-known process called the water vapor-induced phase inversion. In the latter case, absorption of water vapor by a solution film causes a solvent for a polymer to transform into a nonsolvent, resulting in the polymer's precipitation. To our best knowledge, no study has been reported on pore formation due to the water vapor-induced phase separation of a volatile liquid additive.

A DIB molecule has two reactive end groups and thus can be a cross-linker for P2VP. However, because the quaternization reaction was conducted for a short time in an excess of DIB, the probability that both end groups of a DIB molecule would react with pyridine rings of P2VP chains was low. We assumed, therefore, that the DIB molecules were attached mainly by one end, turning qP2VP into a cross-linkable polymer that could be deposited as thin films and afterward cross-linked. The cross-linking was done by annealing the spin-coated films above the glass transition temperature of P2VP (~90−100 °C).[38] We observed no noticeable effect of the temperature annealing on the films' morphology. To estimate the degree of cross-linking, we carried out the control experiment, in which the control qP2VP sample was annealed under the same conditions, i.e., at 120 °C for 48 h. When assessing the results of FTIR measurements of the sample (Figure 1, curves 2 and 3), we found that

the quaternization degree of qP2VP doubled after the annealing. This finding supports our assumption that qP2VP was not cross-linked in the solution. In melt, where the quaternization reaction was thermally activated, the free (unreacted) I-groups of DIB continued binding to qP2VP chains, forming cross-links. The annealing over a long period of time (48 h) ensured the complete conversion of the reactive groups and resulted in the cross-linking degree of ~11% (by number of monomer units). The control experiment also indicates that the S_N2 reaction responsible for cross-linking was dominant, while the concurrent reaction of E2 elimination that leads to the loss of iodine was negligible.

The cross-linked films demonstrated pH-responsive swelling properties. For the experiments, we chose the qP2VP membrane prepared from the primary solution at 55% RH (see Figure 2a). Swelling was studied by carrying out in-situ SPM measurements in a liquid cell. The SPM topography images (Figure 6A,B) reveal a decrease of the pore size that occurred with an increase in acidity of aqueous solutions. The cross-sectional profiles obtained from the images of the membrane under water at pH 2 (see Figure 6B) show that the SPM tip penetrates into the pores less than one-half the depth of the pores. This result suggests that most of the pores were completely closed. We also performed an SPM scratch analysis to measure the thickness of the swollen membrane. The obtained values were used to estimate the swelling degree of the cross-linked qP2VP network. The swelling degree was expressed as a ratio of the swollen and dry membrane thickness and was found to be 1.9 for pH 3 and 2.4 for pH 2. At pH 2, the pyridine rings of P2VP are fully protonized, and the membrane shows the maximum swelling degree. The changes in pore diameter are fully reversible, as was shown by multiple swelling−shrinking cycles (more than 10 times). It is worth noting that strong interactions of qP2VP with Si substrates prevented the films from peeling. We sometimes observed the partial detachment of the membranes after the multiple treatments with acidic water of pH 2. Conversely, the films chemically bound to the substrates through a BDCS monolayer demonstrated excellent stability.

The adhesion of a membrane to a substrate must affect its swelling[39] and the geometry of swollen pores. Since the influence of the substrate weakens with distance, qP2VP can expand more freely to the interior of a pore. As a result, we may assume that the swollen pore will adopt the bottleneck profile, as is schematically shown in Figure 6C.

Conclusion

We have developed a simple, novel method for the fabrication of pH-responsive polymer thin film membranes with submicrometer concave pores. The membranes are prepared from a solution containing qP2VP and DIB, where DIB serves as a pore-forming additive. The pore formation occurs during the spin-coating deposition and requires a humid environment. The DIB content in the solution and the relative humidity are essential parameters controlling the average pore size. The hypothetical scenario of pore formation, which explains the experimentally observed film morphology, involves the condensation of water vapor due to the evaporative cooling of a solution on the substrate, which triggers the phase separation of DIB. After solvent evaporation, qP2VP vitrifies and produces a continuous film around the phase separated droplets. The subsequent evaporation of DIB from the droplets leads to the formation of pores.

In addition, qP2VP membranes can be cross-linked by the temperature annealing. The cross-linked membranes demonstrate pH-dependent swelling, which has a strong impact on the size of pores and thus makes them potentially attractive for size-dependent filtering, drug delivery systems, and sensors.

Acknowledgment. This work was supported by the U.S. Army Research Laboratory's Army Research Office (ARO), the project W911NF-05-1-0339.

References and Notes

(1) Altinkaya, S. A.; Yenal, H.; Ozbas, B. *J. Membr. Sci.* **2005**, *249*, 163−172.
(2) Apel, P. *Radiat. Meas.* **2001**, *34*, 559−566.
(3) Yan, F.; Goedel, W. A. *Adv. Mater.* **2004**, *16*, 911−915.
(4) Yan, F.; Goedel, W. A. *Chem. Mater.* **2004**, *16*, 1622−1626.
(5) Jiang, P.; Hwang, K. S.; Mittleman, D. M.; Bertone, J. F.; Colvin, V. L. *J. Am. Chem. Soc.* **1999**, *121*, 11630−11637.
(6) Cassagneau, T.; Caruso, F. *Adv. Mater.* **2002**, *14*, 34−38.
(7) Park, S. H.; Xia, Y. N. *Adv. Mater.* **1998**, *10*, 1045−1046.
(8) Jiang, P.; Bertone, J. F.; Colvin, V. L. *Science* **2001**, *291*, 453−457.
(9) Imhof, A.; Pine, D. J. *Adv. Mater.* **1998**, *10*, 697−700.
(10) Odom, T. W.; Love, J. C.; Wolfe, D. B.; Paul, K. E.; Whitesides, G. M. *Langmuir* **2002**, *18*, 5314−5320.
(11) Yan, X. H.; Liu, G. J.; Dickey, M.; Willson, C. G. *Polymer* **2004**, *45*, 8469−8474.
(12) Widawski, G.; Rawiso, M.; Francois, B. *Nature (London)* **1994**, *369*, 387−389.
(13) Yabu, H.; Tanaka, M.; Ijiro, K.; Shimomura, M. *Langmuir* **2003**, *19*, 6297−6300.
(14) Maruyama, N.; Koito, T.; Nishida, J.; Sawadaishi, T.; Cieren, X.; Ijiro, K.; Karthaus, O.; Shimomura, M. *Thin Solid Films* **1998**, *329*, 854−856.
(15) Karthaus, O.; Maruyama, N.; Cieren, X.; Shimomura, M.; Hasegawa, H.; Hashimoto, T. *Langmuir* **2000**, *16*, 6071−6076.
(16) Srinivasarao, M.; Collings, D.; Philips, A.; Patel, S. *Science* **2001**, *292*, 79−83.
(17) Li, Q.; Quinn, J. F.; Caruso, F. *Adv. Mater. (Weinheim, Germany)* **2005**, *17*, 2058−2062.
(18) Jenekhe, S. A.; Chen, X. L. *Science* **1999**, *283*, 372−375.
(19) Ulbricht, M. *Polymer* **2006**, *47*, 2217−2262.
(20) Osada, Y.; Honda, K.; Ohta, M. *J. Membr. Sci.* **1986**, *27*, 327−338.
(21) Kontturi, K.; Mafe, S.; Manzanares, J. A.; Svarfvar, B. L.; Viinikka, P. *Macromolecules* **1996**, *29*, 5740−5746.
(22) Mika, A. M.; Childs, R. F.; Dickson, J. M.; Mccarry, B. E.; Gagnon, D. R. *J. Membr. Sci.* **1995**, *108*, 37−56.
(23) Ito, Y.; Park, Y. S.; Imanishi, Y. *J. Am. Chem. Soc.* **1997**, *119*, 2739−2740.
(24) Iwata, H.; Hirata, I.; Ikada, Y. *Macromolecules* **1998**, *31*, 3671−3678.
(25) Peng, T.; Cheng, Y. L. *Polymer* **2001**, *42*, 2091−2100.
(26) Ito, T.; Hioki, T.; Yamaguchi, T.; Shinbo, T.; Nakao, S.; Kimura, S. *J. Am. Chem. Soc.* **2002**, *124*, 7840−7846.
(27) Iwata, H.; Oodate, M.; Uyama, Y.; Amemiya, H.; Ikada, Y. *J. Membr. Sci.* **1991**, *55*, 119.
(28) Park, Y. S.; Ito, Y.; Imanishi, Y. *Langmuir* **1998**, *14*, 910−914.
(29) Yamaguchi, T.; Ito, T.; Sato, T.; Shinbo, T.; Nakao, S.-i. *J. Am. Chem. Soc.* **1999**, *121*, 4078−4079.
(30) Ying, L.; Wang, P.; Kang, E. T.; Neoh, K. G. *Macromolecules* **2002**, *35*, 673−679.
(31) Liu, G. J.; Lu, Z. H.; Duncan, S. *Macromolecules* **2004**, *37*, 4218−4226.
(32) Zhai, G. Q.; Toh, S. C.; Tan, W. L.; Kang, E. T.; Neoh, K. G.; Huang, C. C.; Liaw, D. J. *Langmuir* **2003**, *19*, 7030−7037.
(33) Hester, J. F.; Olugebefola, S. C.; Mayes, A. M. *J. Membr. Sci.* **2002**, *208*, 375−388.
(34) Ly, Y.; Cheng, Y.-L. *J. Membr. Sci.* **1993**, *77*, 99.
(35) Tokarev, I.; Orlov, M.; Minko, S. *Adv. Mater.* **2006**, *18*, 2458−2460.
(36) Stohr, J.; Anders, S. *IBM J. Res. Dev.* **2000**, *44*, 535−551.
(37) Barenbrug, A. W. T. *Psychrometry and Psychrometric Charts*, 3rd ed.; Cape and Transvaal Printers Ltd.: Cape Town, , 1974.
(38) Papadopoulos, P.; Peristeraki, D.; Floudas, G.; Koutalas, G.; Hadjichristidis, N. *Macromolecules* **2004**, *37*, 8116−8122.
(39) Toomey, R.; Freidank, D.; Ruhe, J. *Macromolecules* **2004**, *37*, 882−887.

MA062821F